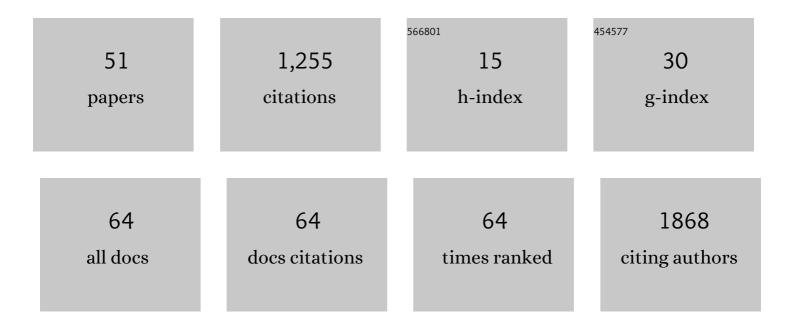
Iman Aganj

List of Publications by Year in descending order

Source: https://exaly.com/author-pdf/4632773/publications.pdf Version: 2024-02-01



IMAN ACANL

#	Article	IF	CITATIONS
1	Characterization Of Spatial Dynamics Of Fmri Data In White Matter Using Diffusion-Informed White Matter Harmonics. , 2021, 2021, 1586-1590.		1
2	Radius-optimized efficient template matching for lesion detection from brain images. Scientific Reports, 2021, 11, 11586.	1.6	2
3	Multi-Atlas Image Soft Segmentation via Computation of the Expected Label Value. IEEE Transactions on Medical Imaging, 2021, 40, 1702-1710.	5.4	8
4	Diffusion-informed spatial smoothing of fMRI data in white matter using spectral graph filters. Neurolmage, 2021, 237, 118095.	2.1	22
5	Conductance-Based Structural Brain Connectivity in Aging and Dementia. Brain Connectivity, 2021, 11, 566-583.	0.8	7
6	Quantification of volumetric morphometry and optical property in the cortex of human cerebellum at micrometer resolution. Neurolmage, 2021, 244, 118627.	2.1	7
7	Cortical Surface-Informed Volumetric Spatial Smoothing of fMRI Data via Graph Signal Processing. , 2021, 2021, 3804-3808.		2
8	Compensatory Brain Connection Discovery in Alzheimer's Disease. , 2020, 2020, 283-287.		7
9	The optical property and morphometry of human cerebellum cortex with automatic serial sectioning polarization sensitive optical coherence tomography (Conference Presentation). , 2020, , .		0
10	Expected Label Value Computation for Atlas-Based Image Segmentation. , 2019, 2019, 334-338.		4
11	Implementation and Validation of a Three-dimensional Cardiac Motion Estimation Network. Radiology: Artificial Intelligence, 2019, 1, e180080.	3.0	29
12	Quantification of structural brain connectivity via a conductance model. NeuroImage, 2019, 189, 485-496.	2.1	15
13	Detecting Structural Brain Connectivity Differences in Dementia Through a Conductance Model. , 2019, , .		5
14	Distinct Patterns of Rich Club Organization in Alzheimer's Disease and Subcortical Vascular Dementia: A White Matter Network Study. Journal of Alzheimer's Disease, 2018, 63, 977-987.	1.2	17
15	as-PSOCT: Volumetric microscopic imaging of human brain architecture and connectivity. NeuroImage, 2018, 165, 56-68.	2.1	50
16	Automatic Verification of the Gradient Table in Diffusion-Weighted MRI Based on Fiber Continuity. Scientific Reports, 2018, 8, 16541.	1.6	0
17	Unsupervised Medical Image Segmentation Based on the Local Center of Mass. Scientific Reports, 2018, 8, 13012.	1.6	59
18	Mid-space-independent deformable image registration. NeuroImage, 2017, 152, 158-170.	2.1	18

Iman Aganj

#	Article	IF	CITATIONS
19	Multimodal Image Registration Through Simultaneous Segmentation. IEEE Signal Processing Letters, 2017, 24, 1661-1665.	2.1	12
20	Functional density and edge maps: Characterizing functional architecture in individuals and improving cross-subject registration. NeuroImage, 2017, 158, 346-355.	2.1	28
21	Accurate High-speed 3D-Registration of EPI vNavs for Head Motion Correction. Proceedings of the International Society for Magnetic Resonance in Medicine Scientific Meeting and Exhibition., 2017, 25, 3944.	0.5	1
22	Effects of Resolution and Registration Algorithm on the Accuracy of EPI vNavs for Real Time Head Motion Correction in MRI. , 2016, 2016, 583-591.		3
23	A Fast Approach to Automatic Detection of Brain Lesions. Lecture Notes in Computer Science, 2016, 10154, 52-61.	1.0	4
24	Superâ€resolution reconstruction in frequency, image, and wavelet domains to reduce throughâ€plane partial voluming in MRI. Medical Physics, 2015, 42, 6919-6932.	1.6	23
25	Noninvasive mapping of pancreatic inflammation in recent-onset type-1 diabetes patients. Proceedings of the National Academy of Sciences of the United States of America, 2015, 112, 2139-2144.	3.3	123
26	An algorithm for optimal fusion of atlases with different labeling protocols. NeuroImage, 2015, 106, 451-463.	2.1	16
27	Avoiding symmetry-breaking spatial non-uniformity in deformable image registration via a quasi-volume-preserving constraint. Neurolmage, 2015, 106, 238-251.	2.1	8
28	Q-Space Modeling in Diffusion-Weighted MRI. , 2015, , 257-263.		2
29	Mid-Space-Independent Symmetric Data Term for Pairwise Deformable Image Registration. Lecture Notes in Computer Science, 2015, 9350, 263-271.	1.0	1
30	Automatic clustering and population analysis of white matter tracts using maximum density paths. NeuroImage, 2014, 97, 284-295.	2.1	31
31	On Removing Interpolation and Resampling Artifacts in Rigid Image Registration. IEEE Transactions on Image Processing, 2013, 22, 816-827.	6.0	28
32	Symmetric non-rigid image registration via an adaptive quasi-volume-preserving constraint. , 2013, 2013, 230-233.		5
33	Motion Detection in Diffusion MRI via Online ODF Estimation. International Journal of Biomedical Imaging, 2013, 2013, 1-8.	3.0	9
34	A 3D wavelet fusion approach for the reconstruction of isotropicâ€resolution MR images from orthogonal anisotropicâ€resolution scans. Magnetic Resonance in Medicine, 2012, 67, 1167-1172.	1.9	19
35	Differential information content in staggered multiple shell hardi measured by the tensor distribution function. , 2011, , .		10
36	Atlas-based fiber clustering for multi-subject analysis of high angular resolution diffusion imaging tractography. , 2011, 2011, 276-280.		10

Iman Aganj

#	Article	IF	CITATIONS
37	Sex differences in the human connectome: 4-Tesla high angular resolution diffusion imaging (HARDI) tractography in 234 young adult twins. , 2011, , .		21
38	A Hough transform global probabilistic approach to multiple-subject diffusion MRI tractography. Medical Image Analysis, 2011, 15, 414-425.	7.0	126
39	Online motion detection in high angular resolution diffusion imaging. , 2011, , .		0
40	3D elastic registration improves HARDI-derived fiber alignment and automated tract clustering. , 2011, , .		5
41	Reconstruction of the orientation distribution function in single―and multipleâ€shell qâ€ball imaging within constant solid angle. Magnetic Resonance in Medicine, 2010, 64, 554-566.	1.9	329
42	Online orientation distribution function reconstruction in constant solid angle and its application to motion detection in HARDI. , 2010, , .		2
43	ODF Maxima Extraction in Spherical Harmonic Representation via Analytical Search Space Reduction. Lecture Notes in Computer Science, 2010, 13, 84-91.	1.0	7
44	Measurement of cortical thickness from MRI by minimum line integrals on soft lassified tissue. Human Brain Mapping, 2009, 30, 3188-3199.	1.9	45
45	ODF reconstruction in q-ball imaging with solid angle consideration. , 2009, 2009, 1398-1401.		41
46	Multiple Q-Shell ODF Reconstruction in Q-Ball Imaging. Lecture Notes in Computer Science, 2009, 12, 423-431.	1.0	14
47	Evaluation of denoising algorithms for biological electron tomography. Journal of Structural Biology, 2008, 164, 7-17.	1.3	38
48	3D priors for scene learning from a single view. , 2008, , .		4
49	Segmentation-free measurement of cortical thickness from MRI. , 2008, 2008, 1625-1628.		3
50	FROM GIGABYTES TO BYTES: AUTOMATED DENOISING AND FEATURE IDENTIFICATION IN ELECTRON TOMOGRAMS OF INTACT BACTERIAL CELLS. , 2007, , .		1
51	REGULARIZATION FOR INVERTING THE RADON TRANSFORM WITH WEDGE CONSIDERATION. , 2007, , .		9